ADVANCED MATERIALS INTERFACES
www.advmatinterfaces.de

Micro–Nano-Texturing Inner Surfaces of Small-Caliber High Aspect Ratio and Superhydrophobic Artificial Vessels using Femtosecond Laser Filamenting Pulses

Xue-Peng Zhan, Yi-Jun Wang, Yue Su, Mu-Tian Li, Hong-Wei Zang, Hong Xia, Huai-Liang Xu, Bin Liu,* and Hong-Bo Sun**

Cardiovascular diseases, the leading cause of death worldwide in the last two decades, are mainly due to the pathological changes inside the heart or blood vessels. Current treatment prescription is to replace obstructed blood vessels by synthetic alternatives, but it can only cure patients effectually when the vessel diameter is larger than a certain value because the cell attachment capacity on a small-caliber artificial vessel is usually unacceptable for long-term patency. Here a femtosecond filamenting laser-based fabrication approach that can produce in situ microstructures on the inner surface of small-caliber tubules is reported. It is shown that the inner-surface fabrication with an aspect ratio as high as 10:1 can be achieved and the processed samples exhibit significant changes in physical properties including topography, roughness, hydrophobicity, as well as in biological property with improved ability for Hela cells to adhere and grow. The results provide a possibility toward fabricating small-caliber artificial vessels that might be suitable for long-term patency use.

1. Introduction

Cardiovascular diseases (CVDs), a class of serious disorders of the heart, the blood vessels or both, are leading causes of premature death worldwide.[1] They result mainly from thrombus formed in the arterial, venous, or capillary circulation, and are commonly treated by inserting vascular prostheses at the occlusive vessel including artificial stents and grafts.[2] Currently, synthetic vessels are in significant demand by clinical patients because proper autologous grafts are very scarce due to the pre-existent vascular diseases.[3] Among the adopted biomaterials such as nylon, dacron, and polyurethane, expanded polytetrafluoroethylene (e-PTFE) is the most commonly used material to make large-caliber diameter artificial vessels in clinical.[4,5] However, because of the low blood compatibility of biomaterials in low flow and high resistance circulation, surface-induced thrombosis and embolization will seriously impair the long-term patency of the synthetic vessel in situations where the graft diameter is normally smaller than 6 mm.

In order to avoid the formation of stenosis and thrombosis, an ideal artificial vessel must possess the biological characteristics similarly to the native ones with sufficient strength, cell compatibility, bioactivity, and biostability.[6] Investigations have demonstrated that surface modification of biomaterial has a profound influence on the interactions between the biological environment and artificial materials.[7–9] Endothelialization of biomaterials, for instance, could be significantly enhanced by altering the physical properties such as porosity, roughness, and hydrophilicity.[10] Therefore, a variety of methods including photochemical technique, micropattern printing, ion-beam irradiation, and plasma treatment[11–14] have been developed so far to modify the surface properties of biomaterials, making them more suitable for cell's adhesion, growth, and proliferation. However, all these methods have been limited to planar surfaces that are not suitable for direct inner-surface modification of artificial vessels.

On the other hand, femtosecond laser-based processing is a powerful 3D fabrication technique that has demonstrated ultrahigh spatial resolution capability approaching to several nanometers as well as broad choices of material species.[15–19] For instance, sharp-spike-shaped black silicon fabricated by femtosecond laser can significantly enhance the absorption of silicon surfaces in a broadband spectrum resulting in

X.-P. Zhan, Y. Su, M.-T. Li, H.-W. Zang, Prof. H. Xia, Prof. H.-L. Xu, Prof. H.-B. Sun
State Key Laboratory of Integrated Optoelectronics
College of Electronic Science and Engineering
Jilin University
Changchun 130012, China
E-mail: huailiang@jlu.edu.cn; hbsun@jlu.edu.cn
Y.-J. Wang, Prof. B. Liu
Department of Hand and Foot Surgery
The First Hospital of Jilin University
Changchun 130021, China
E-mail: kjkliubin@126.com
The ORCID identification number(s) for the author(s) of this article can be found under https://doi.org/10.1002/admi.201801148.

DOI: 10.1002/admi.201801148

 © 2018 WILEY-VCH Verlag GmbH & Co. KGaA, Weinheim

highly efficient and sensitive optoelectronic detectors.[20,21] The processed hydrophobicity of metal material gives rise to a colorful metal with a better corrosion resistance.[22] Micro/nanometer scales of channels or holes with an extended depth on transparent materials have also been fabricated by femtosecond laser irradiation combined with chemical etching.[23–25] However, with this technique, tight focusing is required in most cases to keep high laser intensity. There are lots of difficulties to directly fabricate microstructures on materials with an irregular surface, e.g., curved surfaces on tubules or cylinders. Although by rotating cylinder ceramics, grating-like microgrooves could be produced on the outer surfaces, e.g., for zirconia dental implants in clinical application,[26,27] micro–nano-fabrication on the inner surface of cylinders or tubules especially with small caliber is rarely reported. Recently, femtosecond filamenting pulses, resulting from a dynamic balance between self-focusing and defocusing of plasma, have exhibited a unique ability in fabricating microstructures on irregular surfaces including hemisphere and cylinder metal, remarkably breaking through the bottleneck of the planar techniques.[28,29] More interestingly, it was demonstrated that the filament processing technique can produce almost unique surface properties of black silicon at different standoff distances.[30] The advantages of femtosecond filament processing are mainly based on the almost constant laser intensity clamped inside the filament core with a controllable length from a few centimeters to hundreds of meters.[31] However, this technique has been limited so far to metal and semiconductor materials for standoff micromachining.

In the present study, we explore, as conceptualized in **Figure 1**, the feasibility of the far-field filament technique for in situ fabrication of microstructures on the inner surface of biomaterial tubules to meet the challenge of producing superhydrophobic small-caliber artificial vessels. The surface properties of the processed samples have been characterized by confocal microscopy, scanning electron microscope (SEM), atomic force microscopy (AFM), and contact angle (CA) test. The significant changes on the surface characteristics, including topography, roughness, and wettability, have resulted in a better biocompatibility for Hela cells to adhere and grow.

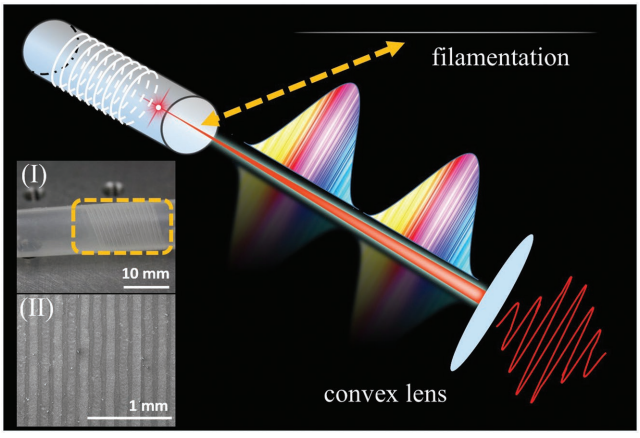

Figure 1. Schematic diagram of femtosecond laser filament processing setup. Inset (I) is the camera picture and Inset (II) is the typical SEM photograph of the fabricated tubules.

2. Results and Discussion

Figure 1 shows a typical photo (inset I) and SEM image (inset II) of the microstructures fabricated on the inner surface of a tubule by femtosecond laser filament processing. An aspect ratio of ≈10:1 has been achieved for the tubule with an inner diameter of 6 mm. During the fabrication, it is found that the aspect ratio is strongly influenced by the operating parameters of the home-built processing system such as the scanning speed and the tilt angle of the tubule with respect to the filament direction. Under the experimental conditions, the produced light intensity inside a filament core in air is clamped to a constant value of 1.3×10^{14} W cm^{-2} for the whole filament length (≈3 cm).[31–33] When the femtosecond laser filament is projected on the tubule surface with an incident angle of ≈84.3° (tilt angle = 5.7°), the light intensity is decreased to ≈1.3×10^{13} cm^{-2} due to the increased spot size of the tilted laser beam on the sample. In addition, the smallest fabrication diameter of the tube with the given tilt angle of ≈5.7° (tan $\theta \sim 0.1$) is estimated, which is ≈453 μm with a fabrication tube length of 2.8 mm. In this estimation the contribution from the energy reservoir that is an important factor for maintaining the filament formation and propagation[31,33] is considered.

To show the above effects, taking polymethyl methacrylate (PMMA) tubules (inner diameter of 10 mm, wall thickness of 1 mm) for instance, we first examine the width and interval of the scanning line as functions of the translation motion and rotation speeds of the tubule. In the experiment, the laser energy of 0.9 mJ and the incident angle of tan $\theta \sim 0.1$ are adopted (see Experimental Section). It can be seen from the inset images of **Figure 2**a that with the same rotation speed of 25 mm s^{-1} the separation distance between adjacent scanning lines increases as the translation motion speed increases, which can be well fitted to a linear function, as shown by the solid line in Figure 2a. The linewidth of each processed line is ≈400 μm (see the insets of Figure 2a), which is mainly determined by the incident angle of the laser filament with respect to the inner surface of the tubule. On the other hand, with a fixed translation motion speed of 37.5 μm s^{-1}, the separation distance between the adjacent scanning lines is inversely proportional to the rotation speed of the tubule (Figure 2b). This is because the increase of the rotation speed will obviously produce more circles at the same time period, giving rise to a decrease of the separation distance. As a result, by optimizing the translation motion and rotation speeds, a uniformed distribution of microstructures on the inner surface of the tubule can be formed. Similar results are also obtained for the tubules with different material and diameters (see Supporting Information).

In order to show the ability of the filament micro–nano-texturing technique for in situ fabrication of small-caliber tubules with diverse materials, we demonstrate in **Figure 3** the confocal microscope images of the surface morphology for the processed silica gel tubules with different rotation speeds of a) 50, b) 75, and c) 100 mm s^{-1}, respectively. In this experiment, the translation

© 2018 WILEY-VCH Verlag GmbH & Co. KGaA, Weinheim

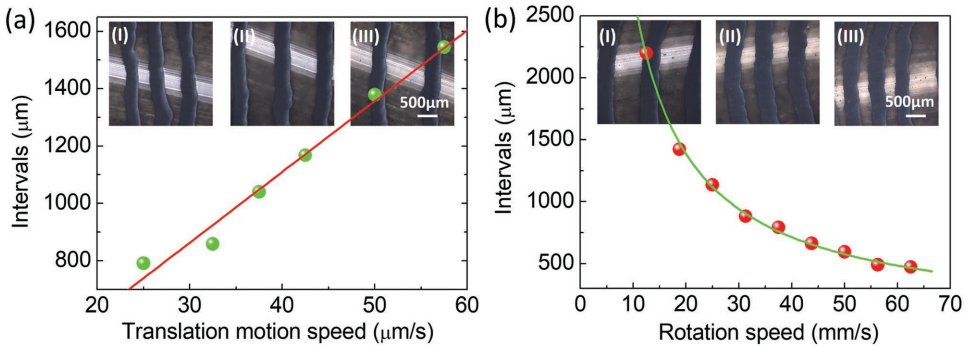

Figure 2. The adjacent line intervals as a function of a): translation motion speed and b): rotation speed. Insets are confocal microscope images of PMMA tubules (d = 10 mm) with different adjacent line intervals.

motion speed is 25 μm s^{-1}, and all the silica gel tubules have a diameter of 6 mm. As shown in Figure 3, a uniformed microstructure could be fabricated on the polymer surface and no directional stress is observed, which is of great importance for microvessels fabrication.[34] Moreover, a high surface area fabrication throughput could be achieved in the femtosecond laser filament fabrication, which is estimated to be ≈1.25 mm^2 per second with a rotation speed (50 mm s^{-1}) and a translation motion speed (25 μm s^{-1}). For comparison, an unprocessed sample is illustrated in Figure 3d. The insets are the zoomed-in images with different resolutions, from which it can be clearly seen that microstructures are formed on the inner surface of the small-caliber tubules.

Since it is difficult to directly and accurately characterize curved surface using SEM and AFM, we cut a large-caliber (25 mm in diameter) silica gel tubule into small pieces with a dimension of 50 mm × 50 mm, whose surface can be roughly regarded as planar. The planar samples are then processed via continuously moving a horizontal stage followed by a vertical shift by using a 2D raster scan system, resulting in controllable separation distance between adjacent scanning lines. The laser energy is ≈0.9 mJ, and the line scanning speed is 125 mm s^{-1}, respectively. The SEM images of the processed planar samples with different line intervals of a) 50, b) 150, and c) 250 μm are shown in **Figure 4**. For comparison, the unprocessed sample is shown in Figure 4d. The insets are the SEM images in a higher resolution. It can be noted that the fabricated surface morphologies shown in Figure 4a–c are different from that in Figure 4d, and that as the line interval decreases, the surface morphology changes from grating shaped to a more uniformed pattern.

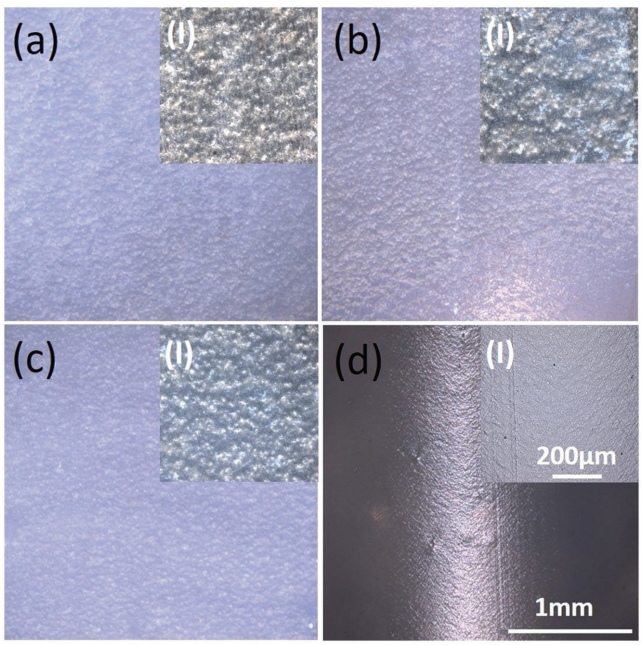

Figure 3. Confocal microscope images of silica gel tubules (d = 6 mm) with different rotation speeds of a) 50, b) 75, and c) 100 mm s^{-1} at the same translation motion speed of 25 μm s^{-1}. d) is the unprocessed sample. Insets are the magnified images.

We also examine, using AFM, the surface roughness of the microstructures of filament processed planar samples under the conditions of 100 μm line interval and 100 mm s^{-1} scanning speed. As shown from **Figure 5**, the roughness of the unprocessed and processed samples is determined to be ≈13.7 (Figure 5a,c) and ≈112 nm (Figure 5b,d) respectively. These results clearly indicate that the unprocessed sample has a relatively smooth surface, and that the laser processing modifies the roughness to a 100 nm scale due to the formation of microstructures on the surface.

For artificial vessels, hydrophobicity is generally required to avoid stenosis and occlusion. To characterize the wettability property of the processed sample surfaces, we measure the water CA of the processed surfaces of silica gel tubule using a Contact Angle Meter. CAs are determined by analyzing the CCD image of a water droplet on the sample surface in a static condition. For the cases of planar (large-caliber) samples (**Figure 6**a,b), the CA of unprocessed sample is ≈98°. With a fixed scanning line interval of 25 μm, the CA is increased to ≈155° with the scanning speed of 50 mm s^{-1}, which slightly decreases from 155° to 145° as the scanning speed increases from 50 to 125 mm s^{-1}. It can also be seen from Figure 6b that with a fixed scanning speed of 125 mm s^{-1}, the CAs of the processed samples fluctuates in the range of 135°–155°. For the cases of the processed small-caliber samples, it can be seen from Figure 6c,d that with different translation motions or rotation speeds the CA values show

© 2018 WILEY-VCH Verlag GmbH & Co. KGaA, Weinheim

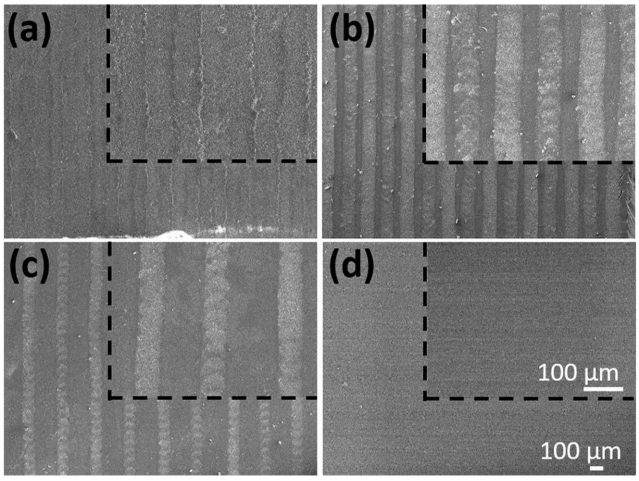

Figure 4. SEM photographs of large-caliber silica gel tubules ($d = 25$ mm) fabricated with different intervals of a) 50, b) 150, and c) 250 μm. The scanning speed is fixed at 125 mm s^{-1}. The insets are the SEM images in a higher resolution.

similar behaviors as those shown in Figure 6a,b, that is, the CAs are increased by ≈45° than that (≈110°) of the unprocessed samples. To test the effect of the fabrication formed debris, which results generally in a negative effect on the fabrication quality,[35] one of the processed sample surfaces was cleaned and then its CA was measured, which decreases from 142° to 137°. Therefore, the randomly deposited debris has a very little influence on the hydrophobic performance. These results clearly show the superhydrophobicity property of the laser modified surfaces.

Furthermore, since the thrombosis and embolization can be significantly reduced if the biological cells could be attached to the vessel surface, the adhesion and growth of Hela cells (similar to endothelial cell) in different groups of the processed sample surfaces are checked. The optical microscope images of cells culture show that Hela cells could grow well on both planar and curved surfaces, showing flat and polygonal epithelial cell morphology (arrow in **Figure 7**). Specifically, for modified planar surfaces, the cell adhesion could be clearly seen in Figure 7 with different scanning line intervals of a) 150, b) 200, and c) 250 μm (scanning speed of 125 mm s^{-1}). The insets are the local images in a higher resolution. Whereas for the unprocessed sample (Figure 7d), there are almost no cells growing on the surfaces regardless of the culture time, suggesting that the surface of the raw material is not suitable for cells to adhere and grow. Similar result is also observed for the small-caliber silica gel samples. Under the same rotation speed of 125 mm s^{-1}, the distribution of the adhered cells with different translation motion speeds 38, 50, and 63 μm s^{-1} are shown in Figure 7e–g. Compared with the unprocessed sample (Figure 7h), the processed surface exhibits a better ability for cells to adhere, grow, and proliferate, indicating the significant improvement of the biocompatibility of the tubule. Because of the little curvature of the small-caliber tubular, microscopic observation is not on the same level with the planar samples, the cell structure shows to be atypical and indistinct (box refers to cells on different levels). Although there are no significant differences in cell growth for modified samples, no cells could be seen to adhere and grow on the surfaces of raw surfaces, regardless of the planar or curved ones.

In the group of the processed materials (planar and curved samples), cell adhesion can be easily and clearly seen on the surfaces, suggesting that the modified surfaces are suitable for cell adhesion after femtosecond filamenting pulses treatment. The cells continue to proliferate with the prolongation of culture time and Hela cells will cover the whole surface as time goes by. The number of cells in the field of view is gradually increased with time until the entire field of view is covered (shown in Figures S3 and S4, Supporting Information), which indicates that the modified surfaces are more biocompatible, enhance the cell adhesion capacity, and provide a suitable condition for cell growth. Furthermore, different scanning speeds and intervals could not change the cell proliferation significantly, showing that different processing parameters does not apparently affect cell growth. However, the unprocessed surface is not suitable for cell attaching and growing since there are barely adhering cells and no significant cell proliferation are observed over time on the surface of nonmodified surfaces.

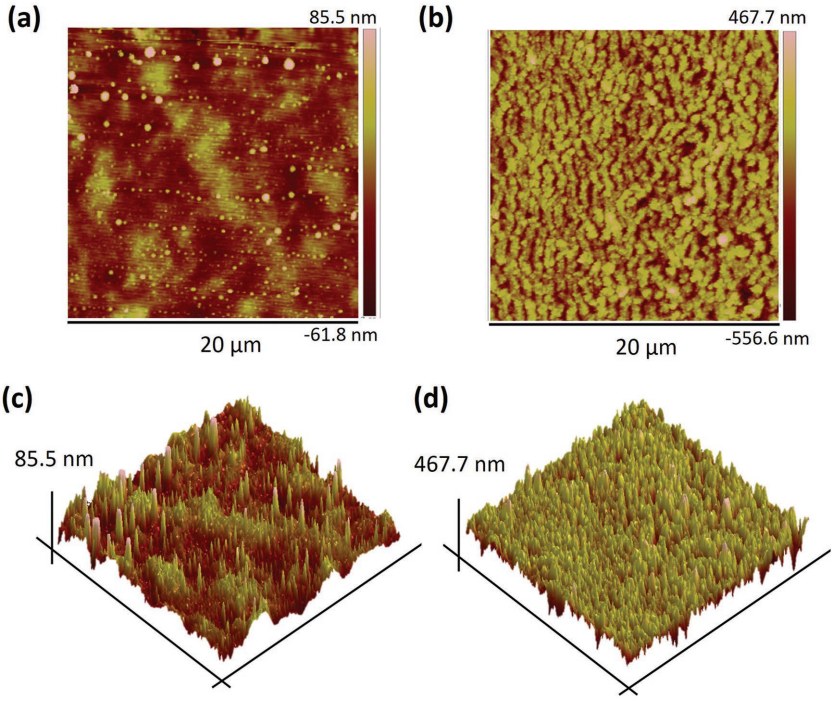

Figure 5. AFM images of the large-caliber silica gel tubules ($d = 25$ mm) with a dimension of 20 μm × 20 μm. The unprocessed sample a,c) and the sample b,d) processed with the scanning speed of 100 mm s^{-1} and interval of 100 μm.

© 2018 WILEY-VCH Verlag GmbH & Co. KGaA, Weinheim

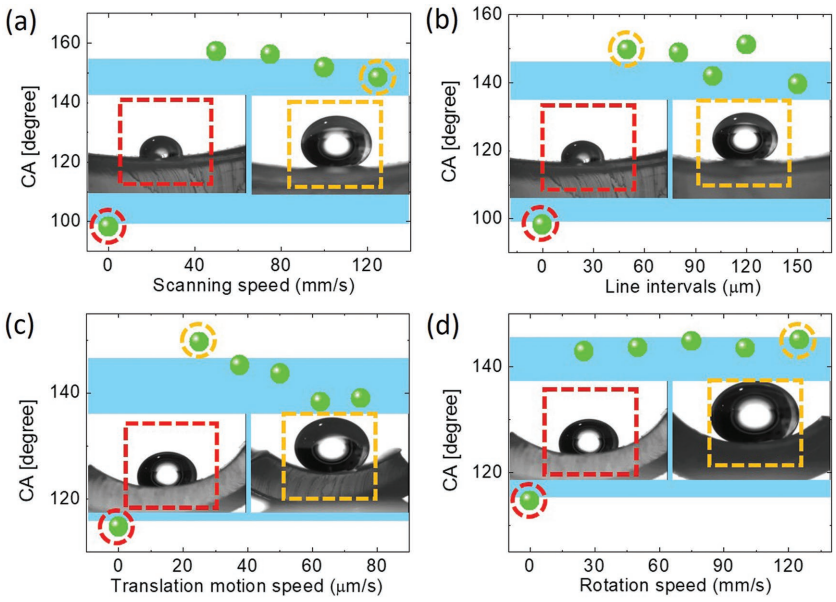

Figure 6. The CAs measured with different a) scanning speeds, b) line intervals, c) translation motion speeds, and d) rotation speeds. a,b) large-caliber tubules (d = 25 mm) and c,d) small-caliber tubules (d = 6 mm).

3. Conclusion

In summary, we have demonstrated the feasibility of in situ fabricating microstructures on the inner surface of artificial vessels via femtosecond laser filament processing, and realized the fabrication of small-caliber tubules with an aspect of ≈10:1. We have further showed that the filament-processed microstructures can strongly change the physical properties of the tubules' inner surfaces including roughness, topography, and wettability, and found that the water CA can reach to ≈150° revealing the superhydrophobic property of the fabricated surface. Furthermore, the processed surface exhibits a better biocompatibility with the enhanced capability for Hela cells to adhere, grow, and proliferate. Our results show the high potential of femtosecond filament processing in standoff micro–nano-texturing of small-caliber artificial blood vessels for CVDs treatment.

4. Experimental Section

Materials: Several commercial tubules of different materials with different inner diameters were employed for the experiments, which included polytetrafluoroethylene (PTFE) tubules (inner diameter of 6 mm) and PMMA tubules (inner diameter of 10 mm) with the same wall thickness of ≈1 mm and length of ≈60 mm, and two kinds of silica gel tubules, whose inner diameters were 25 and 6 mm and the wall thicknesses were 2.4 and 1.6 mm, respectively. The silica gel tubules with the inner diameter of 25 mm could be regarded as planar samples after being cut into pieces and flattened because of its relatively large radius of curvature.

Femtosecond Laser Processing: The experiments were conducted using a Ti: sapphire femtosecond laser amplifier (Spectra-Physics) with a central wavelength of 800 nm, a pulse duration of 35 fs and a repetition rate of 500 Hz. The laser pulse was linearly polarized whose energy was controlled by a half-wave plate and a polarizer inserted in the laser propagation path. The Gaussian beam had ≈1.0 cm in diameter and it was focused by a 1 m lens forming a single filament in air with a length of ≈3 cm and a diameter of ≈100 μm. For planar samples, they were placed at a right angle to the laser filament propagation direction and in the middle of the filament, and processed in a raster scanning system, which was composed of two motorized stages moving along horizontal and vertical directions. For tubule samples, they were mounted firmly in a three-jaw chuck equipped on a moving setup composed of a translation stage and a rotational stage. The translation stage had a step resolution of 2.5 μm, and the rotational stage had a rotational resolution of 0.72 arc second. The translation stage moving

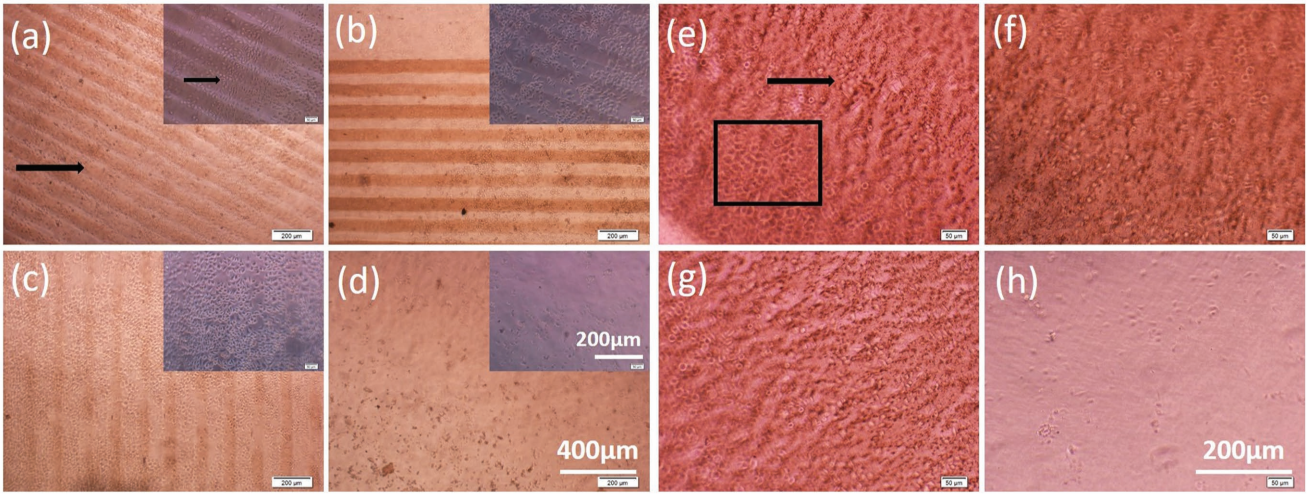

Figure 7. Cell culture results of silica gel tubules processed with different line intervals of a) 150, b) 200, and c) 250 μm for the large-caliber tubules (the scanning speed is fixed at 125 mm s^{-1}) and with different translation motion speeds of e) 38, f) 50, and e) 63 μm s^{-1} for small-caliber tubules (the rotation speed is fixed at 125 mm s^{-1}). d,h) Cell culture result for the unprocessed sample.

© 2018 WILEY-VCH Verlag GmbH & Co. KGaA, Weinheim

along the "z" direction, i.e., the laser propagation direction, provided a "translation motion speed"; meanwhile the rotational stage rotates with the laser beam as the rotation axis giving rise to a "rotation speed." Both the translation and rotation speeds could be precisely controlled by stepper motor controllers. In the measurement, the axis of the tubule cylinders was aligned to have a small tilt angle of $\theta \sim 5.7°$ with respect to the laser propagation direction. The tilt angle played a key role in the determination of the fabricated depth-to-diameter ratio because the laser intensity of the interaction zone was determined by the tilt angle.

Surface Characterization: The morphologies of the unprocessed and processed inner surfaces of tubules were measured by a field SEM (JEOL JSM-7500F) and a confocal laser scanning microscope (LEXT OLS 4100, OLYMPUS) and the surface roughness of the tubule films was characterized by using AFM (Digital Instruments Nanoscope IIIA, Dimension Icon) in the tapping mode. In order to examine the hydrophilicity, the measurement of the CAs were carried out by static conditions sessile drop technique using a Contact Angle Meter SL200B (Solon Tech., Shanghai) at room temperature in air.

Cell Culture: The unprocessed and processed planar and curved pieces were placed in a 24-well cell culture plate and immersed in 75% medical alcohol for 12 h, and then placed in sterile phosphate buffer saline (PBS, Mediatech Inc. USA) for use. Hela cells were thawed, cultured and passaged. Dulbecco's Modified Eagle Medium (DMEM, Thermo Fisher Scientific, China) with 1% double antibiotics (Penicillin-Streptomycin Solution, The first hospital of Jilin University, China), 1% L-G (L- Glutamine, The first hospital of Jilin University, China) and 10% fetal bovine serum (HyClone Laboratories Inc. USA) were used for cell culture. Cells were seeded in the T-25 culture flask, and kept in a humidified cell incubator (Thermo 371. USA) containing 5% CO_2 at 37 °C. The cells in logarithmic growth phase (70–80% adherence rate) were used for cell adhesion experiments.

In the biohazard safety equipment (Thermo 1300 series A2. USA), the cell culture medium in the T-25 flask was discarded and ≈2 mL of PBS is added. Then the flask was rocked and PBS was removed. Trypsin-EDTA (1 mL, 0.25%, HyClone Laboratories Inc. USA) was added for 5 min. 2 mL of cell culture medium was added and dispersed by a pipette over the cell layer surface several times. Then the cell suspension was transferred into a 15 mL centrifuge tubule and centrifugated for 5 min at 4 °C at 1650 rpm (Allegra X-15R Centrifuge, Beckman Coulter, USA). The supernatant was discarded and the cell pellet was resuspended in 1 mL of cell culture medium. In the biohazard safety equipment, samples had been placed in different wells of a 24-well cell culture plate, and 1 mL of DMEM was added into every well allowing the solution to cover the sample surface. Two wells without the samples were as control to observe the cell attachment. 50 µL of Hela cells suspension was added to each well and the cell culture plate was gently shaken before being placed in the cell incubator.

The cell growth of the control wells was checked with an inverted microscope (Olympus IX51. Japan) every 6 h. When most of the cells were already adhered to the wells of Control, the medium was discarded and 1 mL of PBS is added into each well. The surfaces were gently blowing with PBS to wash out the residual cell culture medium. The samples were transferred into the wells of a new cell culture plate in turn with a sterilized tweezer, and 1 mL of preheated DMEM was added to every well. The cultured cells were monitored under the microscope per 12 h.

Supporting Information

Supporting Information is available from the Wiley Online Library or from the author.

Acknowledgements

X.P.Z. and Y.J.W. contributed equally to this work. The work was supported in part by National Natural Science Foundation of China (61625501, 61427816), National Basic Research Program of China (2014CB921302), the Program for JLU Science and Technology Innovative Research Team (JLUSTIRT) (2017TD-21), and Fundamental Research Funds for the Central Universities.

Conflict of Interest

The authors declare no conflict of interest.

Keywords

artificial vessels, femtosecond filamenting pulses, micro–nano-texturing

Received: July 26, 2018
Revised: September 12, 2018
Published online: October 16, 2018

[1] N. Mackman, *Nature* **2008**, *451*, 914.
[2] J. Y. Chen, R. L. Tian, Y. X. Leng, P. Yang, J. Wang, G. J. Wan, A. S. Zhao, H. Sun, N. Huang, *Surf. Coat. Technol.* **2007**, *201*, 6901.
[3] T. C. Rothuizen, F. F. R. Damanik, T. Lavrijsen, M. J. T. Visser, J. F. Hamming, R. A. Lalai, J. M. G. J. Duijs, A. J. van Zonneveld, I. E. Hoefer, C. A. van Blitterswijk, T. J. Rabelink, L. Moroni, J. I. Rotmans, *Biomaterials* **2016**, *75*, 82.
[4] D. Anderheiden, D. Klee, H. Höcker, B. Heller, C. J. Kirkpatrick, C. Mittermayer, *J. Mater. Sci.: Mater. Med.* **1992**, *3*, 1.
[5] C. J. Malm, B. Risberg, A. Bodin, H. Bäckdahl, B. R. Johansson, P. Gatenholm, A. Jeppsson, *Scand. Cardiovasc. J.* **2012**, *46*, 57.
[6] M. S. Kim, G. Khang, H. B. Lee, *Prog. Polym. Sci.* **2008**, *33*, 138.
[7] F. F. R. Damanik, T. C. Rothuizen, C. van Blitterswijk, J. I. Rotmans, L. Moroni. *Sci. Rep.* **2015**, *4*, 6325.
[8] T. W. Chung, D. Z. Liu, S. Y. Wang, S. S. Wang, *Biomaterials* **2003**, *24*, 4655.
[9] Y. C. Huang, C. C. Huang, Y. Y. Huang, K. S. Chen, *J. Biomed. Mater. Res., Part A* **2007**, *82A*, 842.
[10] H. Shen, X. Hu, F. Yang, J. Bei, S. Wang, *Biomaterials* **2007**, *28*, 4219.
[11] V. Gauvreau, G. Laroche, *Bioconjugate Chem.* **2005**, *16*, 1088.
[12] B. Pignataro, E. Conte, A. Scandurra, G. Marletta, *Biomaterials* **1997**, *18*, 1461.
[13] S. G. Lee, E. young An, J. B. Lee, J. C. Park, J. W. Shin, J. K. Kim, *Surf. Coat. Technol.* **2007**, *201*, 5128.
[14] H. R. Lim, H. S. Baek, M. H. Lee, Y. I. Woo, D. W. Han, M. H. Han, H. K. Baik, W. S. Choi, K. D. Park, K. H. Chung, J. C. Park, *Surf. Coat. Technol.* **2008**, *202*, 5768.
[15] Y. L. Zhang, Q. D. Chen, H. Xia, H. B. Sun, *Nano Today* **2010**, *5*, 435.
[16] K. Sugioka, Y. Cheng, *Light: Sci. Appl.* **2014**, *3*, e149.
[17] M. Malinauskas, A. Žukauskas, S. Hasegawa, Y. Hayasaki, V. Mizeikis, R. Buividas, S. Juodkazis, *Light: Sci. Appl.* **2016**, *5*, e16133.
[18] J. Ni, C. Wang, C. Zhang, Y. Hu, L. Yang, Z. Lao, B. Xu, J. Li, J. Chu, *Light: Sci. Appl.* **2017**, *6*, e17011.
[19] L. Wang, Q. D. Chen, X. W. Cao, R. Buividas, X. Wang, S. Juodkazis, H. B. Sun, *Light: Sci. Appl.* **2017**, *6*, e17112.
[20] J. Yang, F. Luo, T. S. Kao, X. Li, G. W. Ho, J. Teng, X. Luo, M. Hong. *Light: Sci. Appl.* **2014**, *3*, e185.
[21] T. H. Her, R. J. Finlay, C. Wu, S. Deliwala, E. Mazur, *Appl. Phys. Lett.* **1998**, *73*, 1673.
[22] R. Fang, A. Vorobyev, C. Guo, *Light: Sci. Appl.* **2017**, *6*, e16256.

 © 2018 WILEY-VCH Verlag GmbH & Co. KGaA, Weinheim

[23] A. Pan, J. Si, T. Chen, Y. Ma, F. Chen, X. Hou, *Opt. Express* **2013**, *21*, 16657.
[24] X. Zhao, Y. C. Shin, *Appl. Phys. A* **2011**, *104*, 713.
[25] B. Mills, D. Kundys, M. Farsari, S. Mailis, R. W. Eason, *Appl. Phys. A* **2012**, *108*, 651.
[26] J. L. Calvo-Guirado, A. Aguilar-Salvatierra, R. A. Delgado-Ruiz, B. Negri, M. P. R. Fernández, J. E. Mate Sanchez de Val, G. Gómez-Moreno, G. E. Romanos, *Clin. Implant Dent. Related Res.* **2015**, *17*, 525.
[27] R. A. Delgado-Ruiz, J. L. Calvo-Guirado, M. Abboud, M. P. Ramirez-Fernandez, J. E. Mate-Sanchez, B. Negri, D. Rothamel, *Clin. Implant Dent. Related Res.* **2014**, *16*, 856.
[28] D. Kiselev, L. Woeste, J. P. Wolf, *Appl. Phys. B* **2010**, *100*, 515.
[29] H. Tao, J. Lin, Z. Hao, X. Gao, X. Song, C. Sun, X. Tan, *Appl. Phys. Lett.* **2012**, *100*, 201111.
[30] X. Zhan, H. Xu, C. Li, H. Zang, C. Liu, J. Zhao, H. Sun, *Opt. Lett.* **2017**, *42*, 510.
[31] M. A. Rodriguez, R. Bourayou, G. Mejean, J. Kasparian, J. Yu, E. Salmon, A. Scholz, B. Stecklum, J. Eisloffel, U. Laux, A. P. Hatzes, R. Sauerbrey, L. Woste, J. P. Wolf, *Phys. Rev. E* **2004**, *69*, 036607.
[32] X. L. Liu, W. Cheng, M. Petrarca, P. Polynkin, *Opt. Lett.* **2016**, *41*, 4751.
[33] H. Xu, Y. Cheng, S. L. Chin, H. Sun, *Laser Photonics Rev.* **2015**, *9*, 275.
[34] S. Juodkazis, *Int. J. Nanomed.* **2012**, *7*, 3701.
[35] M. Malinauskas, S. Rekštytė, L. Lukoševičius, S. Butkus, E. Balčiūnas, M. Pečiukaitytė, D. Baltriukienė, V. Bukelskienė, A. Butkevičius, P. Kuscevičius, V. Rutkūnas, S. Juodkazis, *Micromachines* **2014**, *5*, 839.

 © 2018 WILEY-VCH Verlag GmbH & Co. KGaA, Weinheim